Title

Soil Gas Entry into an Experimental Basement: Model-Measurement Comparisons and Seasonal Effects

Authors

Garbesi, K.
Sextro, R.G.
Fisk, W.J.
et al.

Publication Date

1992-03-01

LBL-31873
UC-402
Preprint

Lawrence Berkeley Laboratory

UNIVERSITY OF CALIFORNIA

ENERGY & ENVIRONMENT DIVISION

Submitted to Environmental Science and Technology

Soil-Gas Entry into an Experimental Basement: Model-Measurement Comparisons and Seasonal Effects

K. Garbesi, R.G. Sextro, W.J. Fisk, M.P. Modera, and K.L. Revzan

March 1992

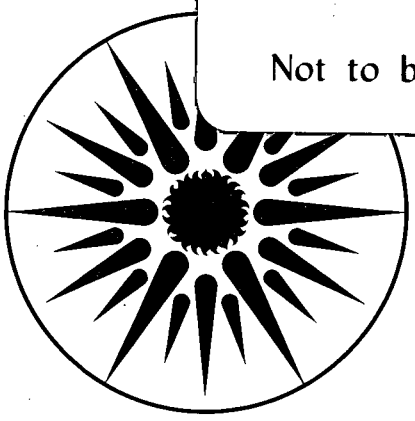

ENERGY & ENVIRONMENT DIVISION

Prepared for the U.S. Department of Energy under Contract Number DE-AC03-76SF00098

DISCLAIMER

LBL-31873

To be submitted to *Environmental Science and Technology*

SOIL-GAS ENTRY INTO AN EXPERIMENTAL BASEMENT: MODEL-MEASUREMENT COMPARISONS AND SEASONAL EFFECTS

K. Garbesi, R.G. Sextro, W.J. Fisk, M.P. Modera, and K.L. Revzan

March 1992

Indoor Environment Program
Energy and Environment Division
Lawrence Berkeley Laboratory
1 Cyclotron Road
Berkeley, California 94720

This work was supported by the Director, Office of Energy Research, Office of Health and Environmental Research, Environmental Sciences Division, and by the Assistant Secretary for Conservation and Renewable Energy, Office of Building and Community Systems, Building Systems and Materials Division of the U.S. Department of Energy (DOE), under Contract DE-AC03-76SF00098.

Abstract

Previous field studies of soil-gas entry into existing houses have found large discrepancies between modeled and measured values of soil-gas entry rate and pressure coupling between house substructures and the soil that could have been explained by inherently poor understanding of complex field sites. This paper reports the results of detailed investigation of soil-gas entry into an extensively instrumented and controlled experimental basement designed for the verification of existing numerical models of soil-gas and radon entry into houses. The experimental design provides greatly reduced uncertainty regarding structure and soil characteristics. Estimates of soil-gas entry based on radon mass-balance in the structure are compared with predictions of a 3-dimensional, steady-state numerical model. This study corroborates the earlier findings of significant model underprediction of soil-gas entry and far-field pressure coupling. Observed soil-gas entry at 21 Pa structure depressurization was 8 times greater than predicted by the model and far-field pressure coupling was as much as 6 times greater than predicted. This suggests that field conditions at the site, and possibly at real houses, are inconsistent with model assumptions, or that typical methods of assessing bulk soil permeability are misleading. A number of hypotheses are raised to explain the discrepancy that will be tested in the future at the experimental facility. The effect of seasonal changes in soil conditions on soil-gas entry is also examined. Despite large seasonal changes in near-surface soil moisture content and air permeability, there is no observable effect on soil-gas entry because critical soil conditions near the soil-gas entry location in the structure floor remain relatively constant.

Introduction

Soil-gas entry into houses has been studied in relation to indoor exposures of humans to radon progeny and volatile organic chemicals (VOC). Advective entry of soil gas is believed to be the dominant source of excessive indoor radon concentrations (1-7), and may be a significant source of indoor exposure to toxic VOC in houses near landfills (8), near leaky gasoline storage tanks, or near other chemical storage or disposal sites. A number of mechanisms can cause the indoor-outdoor pressure difference that drives advective entry: thermal differences between indoors and out, wind loading on the building super-structure, imbalanced building ventilation systems, and barometric pressure fluctuations (9-11).

Numerical modeling and field studies at existing houses have been dominant methods for investigating soil-gas entry. Although a great deal has been learned from these studies, large uncertainties remain. In field studies at real houses, the large size and complex geometries lead to significant uncertainties regarding the transport pathways through the soil and into the structure, significant entry points may even be concealed from view. The pressure differences that drive soil-gas entry are uncontrolled and temporally variable. In addition, at occupied sites, detailed studies are generally impossible because of the invasive nature of the instrumentation required to fully probe the site for necessary information on soil, structure, atmospheric and meteorological conditions.

This paucity of data from thoroughly characterized sites has made it impossible to rigorously test the conceptual model of contaminant entry from soil, or to rigorously validate the numerical models. Yet, without the understanding that could be gained therefrom, the ability to achieve a number of public-health-related policy goals is impaired. Regarding the indoor radon problem in particular, improved understanding would help us to locate houses with the potential for high radon concentrations, obviating the need for costly testing in all homes, to design effective radon mitigation systems for different environments and structures, and to develop rational and cost effective building regulations that minimize indoor exposures.

Yet, there is evidence from a number of studies that our understanding of soil-gas entry into houses might have serious flaws. Comparisons between measurements and the results of numerical and analytical models have indicated significant discrepancies. Nazaroff et al. (6) found disturbance pressures in the soil due to house depressurization 10 times greater than predicted with their analytical model. The numerical modeling of Revzan et al. (12) found that average soil-gas entry measured by Turk et al. (13) exceeded their modeled values by a factor of 4. Similarly, Garbesi and Sextro (14) found measured soil-gas entry rates to be high by a factor of 10, and far-field pressure coupling to be high by a factor of 3, when compared to model results using the standard assumptions of impermeable walls and floor, with

soil-gas entry restricted to a gap in the wall-floor interface, and homogeneous soil. That work indicated that the assumed soil-gas entry pathway and the macroscopic structure of the soil permeability field can have a large effect on the predicted entry rate and pressure field, respectively.

To overcome the large uncertainties inherent in field studies, we have designed and built room-sized experimental structures for the detailed study of radon entry into basements (15). These primarily-below-grade structures are thoroughly instrumented and controlled and have a simple geometry suitable for testing existing numerical models employing the standard assumptions about soil-gas entry. In particular, the structures have impermeable walls and floors, with pressure-driven entry of soil gas restricted to precisely engineered slots in the floors.

This paper discusses research on soil-gas entry carried out at the western-most of two structures located in the Santa Cruz Mountains, California. There are two goals: to compare detailed measurements of soil-gas entry determined from radon mass-balance calculations with predictions of a 3-dimensional finite-difference model that uses measured soil permeabilities as inputs; and to investigate the effects of seasonal changes in soil conditions on soil-gas entry into the structure.

Experimental Methods and Results

This section briefly introduces relevant information about the structure, site, and instrumentation. Then we discuss soil moisture and permeability measurements, parameters that control air transport through soil, and pressure coupling between the structure and the soil, an indicator of the soil-gas transport pathway. Next, the soil-gas entry experiments are described. In each case, we discuss both static results and seasonal trends.

Site and Structure Characterization

The structure is located on the top of a wide, flat ridge in the Santa Cruz Mountains, near Ben Lomond, CA, underneath a canopy of oak trees. The region experiences an average 1.5 m of rainfall annually. A groundwater monitoring well at the site indicates typical ground water levels of 15 m below the soil surface, although, in one measurement made in July of 1991 the water level was only 10 m below the surface. Details on the structure design and instrumentation may be found in Fisk et al. (16). Geological details of the site are described in Flexser et al. (17). Important points are summarized below.

The structure is a single chamber with width, depth, and height of 2.0, 3.2, and 1.9 m, respectively (inner dimensions), about 0.1 m of the walls lying above grade. Built of poured concrete with 0.15-m thick walls and floor, a 12-cm thick gravel layer underlies the floor slab. Inclusion of a gravel layer is a customary construction practice in some areas to facilitate water drainage away from the substructure.

After the structure was built, the excavated region outside the structure walls was refilled with the natural soil; this region is referred to as the *backfill*. Care was taken to repack the backfill soil evenly and similarly to the surrounding soil.

The structure was designed to have minimum uncontrolled leakage from the surface and the soil, having an effective leakage area (ELA) of 0.24 cm^2 as measured on September 29, 1990, with all intentional openings to the soil sealed. ELA is a measure of the equivalent open area that would yield the observed leakage at 4 Pa depressurization (18). The structure pressure is controlled by adjusting the exhaust air flow using a proportional-integral-differential software control loop.

The structure floor includes 6 slots that simulate the shrinkage gap that can develop in real houses at the periphery of poured concrete floors. The smooth-walled slots are 1-m long, 0.003-m wide, 0.15-m deep, and are inset 0.34 m from, and parallel to, the walls, inboard of the wall footer. There are two slots along the longer east and west walls and one each along the north and south walls.

Soil probes, described in Fisk et al. (15), penetrate the structure at 32 locations and are used for measuring pressure differences between the soil and the structure, for sampling ^{222}Rn, and measuring the permeability of the soil to air. The probes are lengths of steel pipe with cylindrical well screen of the same diameter welded near the solid, pointed end for soil gas sampling and pressure measurements. Short, medium, and long probes, having lengths from the outside of the wall to the middle of the sampling screen of 0.50, 1.71, and 2.39 m, penetrate the walls horizontally at three depths below the soil surface: 0.18, 0.8, and 1.6 m, with eight probes of various lengths at each depth. These are referred to as *high-wall*, *mid-wall*, and *low-wall* probes, respectively. Eight probes of different lengths are installed vertically through the floor slab, their sampling screens are located 0.24, 0.50, 1.71, and 2.39 m below bottom of the slab.

Naturally occurring ^{222}Rn in the soil is used as a soil-gas tracer to determine the soil-gas entry rate. Three CRMs (continuous radon monitors) are used to sample ^{222}Rn from air in the structure, slots, and soil probes. Structure air is maintained well-mixed using an oscillating fan, allowing sampling from one location. Slot air is drawn from all 6 slots simultaneously, delivering a single sample to the CRM. Soil air samples are multiplexed from the probes to one CRM. We use the method of Busigin et al. (19) to interpret the CRM data. This is particularly important for the multiplexed probe samples in which large concentration changes are seen by the CRM, since the method corrects for alpha decays from radon daughters left in the scintillation cell from previous gas samples.

There are eight thermocouples sensing soil temperatures, one at each of 4 depths (0.20, 1.04, 1.83, and 2.44 m below the surface) in the backfill region, and four similarly placed sensors located 5 m from the structure. Temperatures inside and outside of the structure are also recorded, along with wind speed, wind direction, and barometric pressure.

Soil Moisture and Soil Air-Permeability

Soil moisture measurements are made using a time domain reflectometer (TDR) (Trase System I, Soil Moisture Equipment Corporation) sampling in two different modes. Grab samples are made at different locations on the same date to determine spatial heterogeneity using both 30-cm- and 15-cm-long probes. In other measurements, temporal changes are captured by leaving the 30-cm probe in place and recording soil moisture twice daily. Based on the manufacturers specifications, the TDR averages moisture in the cylindrical volume defined by the length of the probes and the distance between the two tines (2.5 cm), between which the electromagnetic field is propagated, to ± 2 percent, giving a result in percent water volume per bulk soil volume.

Figure 1 shows soil moisture data from measurements made between November 2, 1990 and October 1, 1991, at a location 6 m north of the structure. The vertical bars indicate the spatial variability in soil moisture, as determined by the sample standard deviation of the measurements made with the same length probe at different locations around the structure on a given date. The solid dots indicate continuous sampling with the 30-cm probe. There is considerable spatial variability in soil moisture content, reflecting heterogeneous drainage characteristics of the soil and soil-surface conditions. Greater spatial variability is observed during the drier time of year, probably reflecting heterogeneity in the soil's capacity to retain water, although this interpretation is somewhat uncertain due to the limited number of grab samples during the wetter periods.

The continuous soil moisture data show a clear seasonal trend. The wet season, from about December to March, has elevated soil moisture at about 35%. Soil moisture then decreases almost monotonically to a dry season low of about 8%, except for the obvious rainfall event on June 26, 1991, during which 1.7 cm of rain fell in one day.

The permeability of the soil to air was measured at each of the soil probe locations on a number of occasions between October 13, 1989 and January 7, 1992. The technique involves drawing a steady flow of soil air from a probe while recording the induced disturbance-pressure difference between the probe and the soil surface. The disturbance pressure is the absolute pressure difference between a point and an undisturbed reference location minus the hydrostatic component of pressure. That is:

$$(1) \qquad P_d(h) = P(h) - P_{ref}(0) - \int_0^h \rho g \, dz \ ,$$

where the reference pressure, P_{ref}, is established at z=0, at the soil surface; the disturbance pressure, $P_d(h)$, is measured at some point in the soil at depth z=h, z being positive downwards; P(h) is the absolute pressure at the same point; $\rho(z)$ is the density of air at depth z, and g is the gravitational constant at the earth's surface. Darcy flow occurs in response to a gradient in the disturbance pressure field, given a Reynold's number less than order one (9).

Assuming Darcy flow of soil gas, the soil permeability (k, in m^2) is determined from the relationship:

$$(2) \qquad k = \frac{Q \mu}{S \Delta P} \ ,$$

where Q is the rate at which soil gas is drawn from the probe in $m^3 \ s^{-1}$, μ is the dynamic viscosity of air (1.75×10^{-5} Pa s at ambient conditions), ΔP is the disturbance pressure difference between the probe tip and the soil surface in Pa, and S is the shape factor. The shape factor was determined by numerical modeling to be independent of depth and proximity to the structure to within 10% for the given locations of the probes (15), and has a value of 0.3 m.

Table I indicates the spatial variability in soil permeability and the effect of seasonal changes in soil conditions. The table gives absolute magnitudes of soil permeabilities for two dates, October 1, 1991, for which we found the highest average permeabilities, and January 7, 1992, for which we found the lowest. The uncertainties in the permeabilities are dominated by environmental noise in the measured disturbance pressures. The data are sorted according to location in the soil, demonstrating that there is some structure in the permeability field. Soil in the backfill region has, on average, somewhat lower permeability than the natural soil, and the near-surface natural soil has somewhat lower permeability than the rest of the natural soil. The range in permeability due to spatial variation is considerably larger than due to seasonal variation (a factor of about 200 vs. a factor of about 4).

To capture how soil permeabilities change with time at different elevations in the soil, the permeabilities in each region (high-wall, mid-wall, low-wall, and sub-slab) are averaged for each date; the averages are then normalized with respect to their April 24th value. The seasonal trends are plotted in Figure 2.

During the period of decreasing moisture content in the surface soil (April to October) average soil permeability in the high-wall and mid-wall increased. Due to evaporative losses from the surface, the

effect is largest in the near-surface soil, where average permeability in October peaked at 1.5 times its April value. In the final measurement made during the rainy season in January 1992, the near-surface soil permeability plummets to 0.34 its initial value. The same effect, but of smaller magnitude, is seen in the mid-wall soil. Little seasonality is seen in the low-wall or sub-slab regions.

Pressure Field

To better understand the soil-gas transport pathways, we measured the disturbance pressure between the structure and the soil at the probe locations. *Pressure coupling* is the fraction of the total structure depressurization that is seen at a given point in the soil (the disturbance pressure in the soil divided by the disturbance pressure at slab level in the basement). We report pressure coupling rather than disturbance pressures, since, given Darcy flow and negligible flow resistance through the slots relative to the soil, pressure coupling should be independent of the applied pressure in the structure.

The pressure coupling for a probe at level j is calculated using:

$$(3) \qquad PC_j = \frac{\Delta P_{ref} - \Delta P_j - [\rho(T_{soil})_{h/2} - \rho(T_{in})]\, g\, h_j}{\Delta P_{ref}} .$$

In this case the reference (z=0) is taken at slab level with z positive upwards, and

$\Delta P_{ref} = P_{in,z=0} - P_{\infty,,z=0}$	(the reference pressure-difference measured at slab level between the structure and a point in the soil sufficiently far away not to be disturbed by the structure, Pa)
$\Delta P_j = P_{in,z=j} - P_{soil,z=j}$	(the soil-to-structure pressure difference measured at a probe on level j, Pa)
h_j	(height of the jth level above z=0, floor-slab level, m)
$\rho(T_{soil})_{h/2}$	(the density of air at soil temperature at elevation h/2 at the probe's distance from the structure, kg/m^3)
$\rho(T_{in})$	(the density of air at the structure temperature, kg/m^3)
g	(gravitational acceleration at the earth's surface, 9.8 m/s^2)

Figures 3 and 4 show north-south and east-west cross sections of the Ben Lomond site, indicating the pressure coupling measured on May 4, 1991 and on Sept 25, 1991. To reduce uncertainties due to the effect of wind on the near-surface pressure transducers, the data were taken from periods with the same low, average wind speeds (0.3 $m\ s^{-1}$). For these wind speeds the accuracy of the measurement is limited by the instrumental uncertainty of the pressure transducers, and is 4% or less for all measurements.

Two features of the pressure fields stand out: First, the pressure coupling in the two experiments is remarkably similar. This implies that the pressure field is insensitive to significant seasonal changes, on the order of 60%, in near-surface soil permeability. Second, over-all, the pressure field appears quite symmetric around the structure, indicating that the soil permeability field and the soil-gas flow field are also relatively symmetric on the large scale. A notable exception to the large-scale symmetry is observed in the medium length probe on the west side of the structure, which showed significantly larger coupling than its neighbor nearer the structure wall. This result has appeared consistently in numerous pressure measurements made in the past two years. It suggests the existence of a preferred flow path running between or near the probe tip and the gravel.

Soil-gas Entry

A number of experiments were conducted to investigate advective entry of soil gas into the structure during constant structure depressurization. A steady-state mass balance of ^{222}Rn in the structure was used to calculate the soil-gas entry rate. Radon sources include advective entry through the slots, diffusive entry from and through the walls and through the slots, and unintentional, non-slot leakage below-grade. The contribution of radon from outdoor air is negligible. Sinks include losses by ventilation and decay. With the sources and sinks given in the order mentioned, the mass balance equation is:

$$(4) \qquad Q_{sl}R_{sl} + S_d + Q_{ns}R_{ns} = R_{in}\,Q_{ex} + R_{in}\lambda\,V \;.$$

where Q_{sl} and Q_{ns} are the soil-gas flow rates through the slots and non-slot leaks ($m^3\ s^{-1}$); R_{sl} and R_{ns} are the associated ^{222}Rn concentrations (Bq m^{-3}); S_d is the total diffusive contribution (Bq s^{-1}); R_{in} is the ^{222}Rn concentration in the structure (Bq m^{-3}); Q_{ex} is the exhaust flow from the structure ($m^3\ s^{-1}$); λ is the decay constant of ^{222}Rn ($2.1 \times 10^{-6}\ s^{-1}$); and V is the structure volume (13.4 m^3).

Some of the parameters in Equation 4 (R_{in}, R_{sl}, Q_{ex}) are measured during the advection experiments, others are determined from earlier measurements. S_d, the sum of ^{222}Rn entering by diffusion from and through the walls and through the slots, is estimated from charcoal canister measurements of ^{222}Rn fluxes made at 6 different locations in the other structure at the same site and was determined to be 300 Bq hr^{-1}. The contribution of diffusion through the slots is calculated using Fick's law and the measured concentration difference across the slots. In general, the total contribution from diffusion during an advective entry experiment is small relative to the advective component. For example, in an experiment discussed below in which the structure was held at -21 Pa, about 20 Bq s^{-1} entered by advection of ^{222}Rn, while only about 0.08 and 0.03 Bq s^{-1} entered by diffusion of ^{222}Rn through and from the walls and through slots, respectively--contributions of less than 0.5%.

The soil-gas entry rate is given by the sum of Q_{sl} and Q_{ns}. An upper bound was determined for Q_{ns} by an experiment in which we depressurized the structure by 100 Pa with the slots sealed. In that case, Q_{sl} in Equation 4 is zero, and we can solve for Q_{ns} given R_{ns}. Since we have no way of knowing the spatial distribution of possible non-slot leaks we make two assumptions. Our best estimate assumes that non-slot leakage is distributed uniformly over the walls and floors, so that R_{ns} is given by the area-weighted-average of ^{222}Rn concentrations measured in the high-wall, mid-wall, low-wall, and sub-slab probes nearest the structure. A highest estimate of the non-slot entry is obtained by assuming that all leakage occurs in the high-wall region where the ^{222}Rn concentrations are lowest. The best and maximum estimates of non-slot leakage with the slots sealed are 0.13 and 0.40 L min^{-1} Pa^{-1} ($2.2x10^{-6}$ and $6.7x10^{-6}$ m^3s^{-1} Pa^{-1}), respectively.

The values of Q_{ns} and R_{ns} for the advection experiments with the slots open is modified to account for the change in the across-shell driving pressures relative to when the slots are sealed. Because of the mitigating effect of flow through the slots, given the same structure depressurization, points closer to the slots have considerably reduced driving pressures with the slots open. Therefore, the best-estimates of both Q_{ns} and R_{ns} during depressurization with slots open are weighted by the relative driving pressures and concentrations measured in each of the four regions (high-wall, mid-wall, low-wall, and slab) assuming that the leakage area is uniformly distributed over the four regions. Given our best estimates of Q_{ns} and Q_s, non-slot below-grade entry constitutes about 8% of total soil-gas entry.

Figure 5 shows the maximum, minimum, and best estimates of soil-gas entry rate vs. depressurization based on the radon balance given in Equation 4. The maximum and minimum values of Q_s incorporate both the maximum uncertainty in Q_{ns} and the propagation of error from other measured parameters. As expected for Darcy flow through soil, the relationship is linear ($r^2 = 0.995$ for the weighted fit). Notice that there is no significant difference between the entry measured in May and September, 1991. We conclude, therefore, that, at this site, seasonal changes in soil characteristics do not result in significant changes in soil-gas entry that are sustained over time. At sites that receive sufficiently heavy and frequent rain, such that much of the soil horizon becomes saturated at once, significant suppression of soil-gas entry might occur.

Numerical Modeling and Comparison with Experiments

This section describes the use of a 3-dimensional finite-difference model used to simulate the conditions of the advective entry experiment of September 25, 1991, given the average regional soil permeabilities measured on October 1, 1991, as inputs. The model predictions of pressure coupling and soil-gas entry are compared with the results of experiments described in the previous section.

Based on a code written by Loureiro et al. (20), the model was designed to simulate soil-gas and radon transport at under steady-state conditions, in three dimensions, providing predictions of the soil pressure field and soil-gas entry rate. The model assumes isothermal conditions and Darcy flow, and restricts soil-gas entry to occur via gaps in the structure floor (the walls and floors being otherwise impermeable). The gaps are assumed to provide no resistance to flow, a reasonable assumption given the slot width in the structure. The soil is assumed to be piece-wise homogeneous and isotropic. The porosity, permeability, and soil density can vary among regions.

To validate the physics of the numerical model we compared the soil-gas entry prediction of a simplified, cylindrical version of the 3-dimensional Cartesian model used here with the analytical solution for flow into a horizontal buried cylinder. The analytical solution uses Bi-polar coordinates, as described in Morse and Feshbach (21). Soil-gas entry predictions of the cylindrical model were consistently about 8% higher than predictions of our Cartesian model (12). The entry prediction of the Bi-polar analytical model was modified to mimic the geometry of entry into the simple structure simulated in the cylindrical model by ignoring flow entering from the upper hemisphere, which is blocked by the structure. The prediction of the Bi-polar model exceeds that of the cylindrical model by no more than 25%, and the discrepancy is considerably smaller if we acknowledge that flow coming from the slab-side quadrant would be considerably diminished by the presence of the slab. The soil-gas entry prediction of the Bi-polar model therefore exceeds that of the Cartesian model by no more than 33%--a crude validation that the model simulates the physics of the assumed entry conditions correctly.

The model simulates flow in a quarter block of soil (for example, from the center of the structure to the North, and from the center of the structure to the east). Symmetry is assumed in opposing quadrants. For the purpose of the modeling, the soil at the Ben Lomond site was broken down into the following regions: upper backfill, between the soil surface and 1.3-m depth; lower backfill, between 1.3 and 1.9 m; natural surface-soil from the surface to 0.5 m depth; natural soil lying below 0.5 m depth; and sub-slab gravel extending 0.10 m below the floor slab and lying within the wall footers. Average soil permeabilities were determined for each region using the data for October 1, 1991, in Table I. Gravel permeability, was determined using laboratory soil-column measurements and was found to be 2.0×10^{-8} m^2 (15).

Figures 3 and 4 compare the measured and modeled pressure coupling. Predictions at sub-slab probes agree well with the measured values, especially near the gravel layer. At the low-wall level, however, there is a significant discrepancy between the modeled and measured values. Moreover, the relative magnitude of this discrepancy increases as we move toward the soil surface. Although this discrepancy

is greatest in the near-surface soil, the experimental uncertainty is also larger there, so our confidence in our estimation of the magnitude of the discrepancy is lower than for the mid- and low-level soils.

Particularly notable is the discrepancy between the measured and predicted pressure coupling in the far-field soil at the slab and mid-wall level. There, observed coupling is 3 to 6 times larger than the model predicts. The discrepancy is even larger in the anomalous medium-length probe on the west side of the structure that was mentioned earlier. That probe violates the predicted trend of higher pressure coupling existing nearer the structure walls. This violation is also consistently apparent in the near-surface probes, but the relative uncertainties in the measured values are considerably larger there.

The higher-than-expected pressure coupling observed in the far-field raised the possibility of the existence of a high permeability zone occurring in a sleeve around the probe due to disturbance during probe installation. Such a zone would make the pressure at the probe tip reflect the near-wall, highly-coupled region. To test this possibility, thin open-end probes were installed vertically from the soil surface at horizontal distances corresponding to the existing medium and long probes. Pressure coupling measured with these probes agreed well with the results of measurements made with the permanently installed probes.

Figure 5 indicates the soil-gas entry rate predicted by the model for the conditions of the September 25, 1991, advection experiment, based on the permeabilities measured at the soil probes, and extrapolated to other driving pressures assuming the same soil conditions. The model under-predicts the best estimate of soil-gas entry made using Equation 4 by a factor of 8, predicting entry of only 2.6 L min^{-1} ($4.3x10^{-5}$ m^3 s^{-1}) relative to the radon-balance estimate of 21 L min^{-1} ($3.5x10^{-4}$ m^3 s^{-1}) . Even the minimum radon-based estimate of soil-gas entry of 15 L min^{-1} ($2.5x10^{-4}$ m^3 s^{-1}) is a factor of 6 higher than predicted by the model.

To further investigate the nature of this discrepancy, we ran the model again at the same structure pressure, but using the highest values of soil permeabilities measured in each soil region, rather than the average. At 7 L min^{-1} ($1.2x10^{-4}$ m^3 s^{-1}), the model prediction is still a factor of 3 below the best radon-balance estimate of soil-gas entry, and a factor of 2.6 below the minimum estimate. The possible existence of non-Darcy flow near the soil-gas entry locations was dismissed as a possible explanation, since the intertial effects of non-Darcy flow increase the effective soil resistance, thereby suppressing, not enhancing, the entry-rate.

As an additional check on the performance of our numerical model, we compared the predictions of soil-gas entry and pressure coupling of the simplified cylindrical modeled derived from it (discussed in

paragraph 3 of this section) with results of an independently developed model and measurements reported by Andersen (22). Again, regionally-averaged measured permeabilities were used as inputs to the model. Andersen's measurements were made at a small test structure, 0.5 m deep, that like our structure, is underlain by gravel. Both Andersen's and our model agreed well with pressure coupling measured 1.2 m from the small test structure wall and 0.26 m below the soil surface, with 0.6%, 0.7%, and 0.5% coupling predicted and measured, respectively. When scaled to the small test structure, this is the vicinity in which our model gave the worst agreement with measurements made at the Ben Lomond site. Both of the models, however, underpredict the measured soil-gas entry rate at -10 Pa depressurization by about a factor of about 20. As with our model, even when Andersen used the highest measured permeabilities for the soil, the model still underpredicted the measured entry rate. The fact that pressure measurements agree with the model whereas entry measurements do not is an indication that the sources of the two discrepancies found in the Ben Lomond measurements may not be the same. This discussed in greater detail below.

Discussion

There are three key findings of this paper: (1) The observed soil-gas entry rate exceeds that predicted by the numerical model by a factor of 8, given regionally averaged inputs of measured soil permeabilities. (2) Similarly, the observed pressure coupling between the structure and the far-field soil exceeds the model predictions. This was most evident in the mid- and low-wall-level soil 2 m from the structure, where measured values exceeded predicted values by factors of approximately 6 and 3, respectively. (3) The soil-gas entry rate as a function of structure depressurization was insensitive to reasonably large seasonal changes in near-surface soil permeability.

The source of the model-measurement discrepancies of soil-gas entry and pressure coupling may well not be the same, since these parameters can vary independently, as the following example illustrates: Given that the slots provide insignificant resistance to flow--a good assumption in the present case--if soil permeability in all regions is doubled, the predicted soil-gas entry rate will also double, but the pressure coupling will be unchanged. We offer hypothesis to explain the model-measurement discrepancies in soil-gas entry and pressure coupling below.

Underprediction of soil-gas entry could result from systematic bias in the soil permeability measurements or from the existence of high-permeability flow paths not detected by our network of probes. Inter-comparison of permeability tests made using different types of in-situ probes have agreed quite well, giving us some confidence in the probe measurements and their interpretation. We are currently developing an apparatus for making absolute calibrations of the in-situ measuring devices that will resolve the question of bias.

Preferred flow paths might occur as a result of the difference in the physical properties of the soil and structure walls and floor, yielding a thin high-permeability sleave around the structure, or as a result of burrowing by soil fauna or the growth of tree roots. Indeed, animal burrows were observed down to a depth of 10 feet in a trench dug approximately 20 m south-east of the structure, and 70 roots were observed in an area of about 4 m^2 (22). A high permeability flow path or channel between the gravel and the probe tip could explain the anomalously high pressure coupling observed in the medium-length probe on the west side of the structure.

More study will be required to determine whether the presence of one or more channels of this kind could explain the observed soil-gas entry rate while only disturbing the pressure field in a small region of the soil. If spatially infrequent, preferred flow paths are the explanation for the underprediction of soil-gas entry, then using probe techniques to assess the radon entry potential into homes, as previously suggested (24), could yield significantly misleading results since it is impractical to probe complex field sites even as thoroughly as this controlled site. Inaccurate estimates of bulk soil permeability would be most probable in houses with below-slab gravel since the gravel acts as a plenum communicating structure depressurization to a significantly larger region of soil than would cracks or gaps alone, increasing the probability of intercepting spatially infrequent, high-flow channels. Steady-state experiments planned at the second structure at the same site, which has no gravel under the slab, should help resolve this question.

Two mechanisms that could explain the underprediction of the horizontal extension of the pressure field are anisotropy or heterogeneity of soil permeability. Anisotropy would require higher horizontal than vertical permeabilities. Heterogeneity could spread the pressure field by soil layering (14) or if soil permeability increased significantly with increasing distance from the structure. Observable regional differences in soil permeability were included in the model but did *not* produce the observed pressure field. It is possible that our network of soil probes do not capture the existence of a thin but important layer with different soil permeability. This appears unlikely, however, because, although there was indication of physical and chemical changes in soil with depth during soil excavation (17), permeability measurements made on soil cores sampled from difference horizons did not indicate the presence of such a layer (25). A number of experiments are planned to test these hypotheses including probe-to-probe tests of dynamic pressure signals and soil-gas tracer experiments.

The insensitivity of soil-gas entry to significant seasonal changes in near-surface soil permeability can be explained by the fact that the air permeability of much of the soil-gas transport path is unchanging during the year. Furthermore, because the soil-gas velocity field converges toward the gravel, the net

permeability of the soil is most strongly influenced by conditions near the gravel, where average permeability remains relatively constant for several reasons. The region is somewhat protected by the structure; water leached to the deep soil is channeled and dispersed, increasing the spatial variability of permeability and reducing the average moisture content; in addition, loss of water to the surface from evaporation and transpiration reduces transport of water to the deep soil.

and because soil water transport to the deep soil is reduced by evaporation from the surface. The gravel itself plays an insignificant role in determining the net permeability of the soil pathway because its permeability is so much higher than that of the natural soil and should remain fairly constant since its water retention potential is minimal.

Conclusions

Experiments were conducted at an extensively instrumented structure designed for the study of soil gas and radon transport into basement structures, in particular for the validation of existing numerical models. Experiments on soil-gas entry and pressure coupling between the structure and the soil as a function of structure depressurization were compared with the results of a 3-dimensional model of soil-gas transport. Our results corroborate the findings of field studies conducted at existing houses of significant model-measurement discrepancies. The models significantly underpredict soil-gas entry rate as a function of structure depressurization and, to a lesser extent, also underpredict pressure coupling. The model-measurement discrepancy of the soil-gas entry rate found in the current study is supported by a similar discrepancy reported by Andersen (22) in comparisons of measurements made at a small test structure with an independently developed numerical model.

The fact that this model underprediction persists despite significant reduction of the uncertainties to model inputs provided by the controlled and extensively monitored experimental structure, suggests the possibility that conditions at this site, and possibly at real houses, are inconsistent with the model assumptions, or that the typical method of assessing regional soil permeability (an input to the model) can be misleading. This work indicates possible sources of these discrepancies that will be tested at the site in the future.

Resolving these discrepancies at the Ben Lomond site would improve our understanding of the entry of contaminant-bearing soil gas into real houses. In particular, it would provide valuable information for locating houses with the potential for high radon concentrations, for designing effective radon mitigation systems, and for developing rational and cost-effective guidelines for house construction that minimize indoor exposures to radon progeny and other contaminants.

Investigation of the effect of seasonal changes in soil moisture and soil permeability found no measurable seasonal change in soil-gas entry as a function of structure depressurization or in pressure coupling between the structure and the floor, despite large seasonal changes in near-surface soil conditions due to significant temporal variability in precipitation. This was evidently because soil conditions near the entry slots in the floor slab are relatively constant. This suggests that, at least in climates lacking extreme and sustained seasonal changes in soil conditions, the major factor affecting advective entry of contaminants from the soil into basements should be changes in driving pressures due to variation in indoor-to-outdoor temperature differences, in HVAC operation and wind speed, and possibly in patterns of barometric pressure fluctuation. Structures for which entry typically occurs close to the surface, such as slab-on-grade or crawl-space houses, have greater potential to be affected by seasonal changes in soil conditions. In addition, houses in extreme climates, particularly those where the soil freezes seasonally, might see significant seasonal changes in soil-gas entry.

Acknowledgements

The authors thank C.E. Andersen, Y.C. Bonnefous, C. Khalizadeh, D.D. Nesbitt, T. Nuzum, and A.R. Smith for technical assistance, and J.C. Little, W.W. Nazaroff, and Y.W. Tsang for their critiques of the paper. We are also grateful to the California Department of Forestry and the Ben Lomond Nursery for their hospitality at the field site.

Literature Cited

(1) Bruno, R.C. *J. Air Pollut. Control Assn.* **1983,** 33, 105-109.

(2) Akerblom, G.; Anderson, P.; Clavensjo, B. *Radiat. Prot. Dosim.* **1984,** 7, 49-54.

(3) Nero, A.V.; Nazaroff, W.W. *Radiat. Prot. Dosim.* **1984,** 7, 23-39.

(4) Nazaroff, W.W.; Doyle S.M. *Health Phys.* **1985,** 48, 265 - 281.

(5) Sextro, R.G.; Moed, B.A.; Nazaroff, W.W.; Revzan, K.L.; Nero, A.V. (1987) In *Radon and Its Decay Products: Occurrences, Properties, and Health Effect;* Hopke, P., Ed.; ACS Symposium Series 331; American Chemical Society: Washington D.C.; Chapter 2.

(6) Nazaroff, W.W.; Lewis, S.R.; Doyle, S.M.; Moed, B.A.; Nero, A.V. *Environ. Sci. Technol.* **1987,** 21, 459-466.

(7) Turk, B.H.; Prill, R.J.; Grimsrud, D.T.; Moed, B.A.; Sextro, R.G. *J. Air Waste Mange. Assoc.* **1990,** 40, 498-506.

(8) Hodgson, A.T.; Garbesi, K.; Sextro, R.G.; Daisey, J.M. *J. Air Waste Mange. Assoc. In press,* 42(3).

(9) Nazaroff, W.W.; Moed, B.A.; Sextro R.G. In *Radon and Its Decay Products in Indoor Air*, Nazaroff, W.W.; Nero, A.V., Eds.; Wiley: New York, 1988; Chapter 2.

(10) Narasimhan, T.N.; Tsang, Y.W.; Holman, H.Y.*Geophys. Res. Lett.* **1990,** 17, 821 - 824.

(11) Tsang, Y.W.; Narasimhan, Y.W. *Effects of Periodic Atmospheric Pressure Variation on Radon Entry into Buildings;* Lawrence Berkeley Laboratory: Berkeley, CA, 1991; LBL-31164,

(12) Revzan, K.L.; Fisk, W.J.; Gadgil, A.J. *Modeling Radon Entry into Houses with Basements: Model Description and Verification;* Lawrence Berkeley Laboratory: Berkeley, CA, 1991; LBL-27742,

(13) Turk, B.H.; Prill, R.J.; Grimsrud, D.T.; Moed, B.A.; Sextro, R.G.*Radon and Remedial Action in Spokane Valley Homes, Volume 1: Experimental Design and Data Analysis;* Lawrence Berkeley Laboratory: Berkeley, CA, 1987; LBL-23430,

(14) Garbesi, K.; Sextro, R.G.*Environ. Sci. Technol.* **1989,** 23, 1481-1487.

(15) Fisk, W.J.; Modera, M.P.; Sextro, R.G.; Garbesi, K.; Wollenberg, H.A.; Narasimhan, T.N.; Nuzum, T.; Tsang, Y.W. *Radon Entry into Basements: Approach, Experimental Structures and Instrumentation of the Small Structures Research Project;* Lawrence Berkeley Laboratory: Berkeley, CA, 1992; LBL-31684,

(16) Fisk, W.J.;, Flexser, S.; Gadgil, A.J.; Holman, H.Y.; Modera, M.P.; Narasimhan, T.N.; Nuzum, T.; Revzan, K.L.; Sextro, R.G.; Smith, A.R.; Tsang, Y.W.; Wollenberg, H.A. *Monitoring and Modeling for Radon Entry into Basements: A Status Report for the Small Structures Project;* Lawrence Berkeley Laboratory: Berkeley, CA, 1989; LBL-27692.

(17) Flexser, S.; Wollenberg, H.A.; Smith, A.R. *Distribution of Radon Sources and its Effect on Radon Emanation in Granitic Soil at Ben Lomond;* CA; Lawrence Berkeley Laboratory: Berkeley, CA, 1992; LBL-31915,

(18) Sherman, M. In *Energy Sources: Conservation and Renewables;* American Institute of Physics: New York, N.Y., 1985.

(19) Busigin, A.; Van der Vooren; A.W.; Phillips, C.R. *Health Phys.;* **1979,** 37, 659-667.

(20) Loureiro, C.O.; Abriola, L.M.; Martin, J.E.; Sextro, R.G. *Environ. Sci. Technol.;* **1990,** 24, 1338-1348.

(21) Morse, P.M.; Feshbach, H. *Methods of Theoretical Physics, Vol.2.;* McGraw-Hill: New York, 1953, 1210-1211.

(22) Andersen, C.E. *Entry of Soil Gas and Radon into Houses;* Ph.D. Dissertation, Riso National Laboratory: Roskilde, Denmark, 1992; Riso-R-623(EN).

(23) H.A. Wollenberg, personal communication, Feb. 20, 1992.

(24) Nazaroff, W.W.; Sextro, R.G. *Environ. Sci. Technol.;***1989,** 23, 451-458.

(25) S. Flexser, personal communication, Feb. 18, 1992.

Figure Captions

Figure 1. Grab samples and continuous measurements of soil moisture around the Ben Lomond structure. The vertical bars on the grab sample data show spatial variability as indicated by the sample standard deviation of measurements made on a single day at *n* different locations.

Figure 2. Seasonal trends in average air-permeabilities of the soil in the high-wall, mid-wall, low-wall, and sub-slab regions. The averaged values are normalized with respect to their value on April 24, 1991. Only probes with complete data sets are included (7, 8, 5 , and 4 probes in the high-, mid-, low-, and sub-slab- levels, respectively). Vertical bars indicate the standard error in the mean values.

Figure 3. A north/south cross section of the site showing measured and predicted pressure coupling at the indicated probe locations. Measurements were made on May 4, 1991, and September 25, 1991, at 19 and 21 Pa structure depressurization, respectively, and have an uncertainty of ±4%. The numerical model was run given regional average permeabilities measured on October 1, 1991, and assuming 21 Pa structure depressurization.

Figure 4. A east/west cross section of the site showing measured and predicted pressure coupling at the indicated probe locations. Measurements and modeling are as in Figure 3.

Figure 5. Soil-gas entry rate vs. structure depressurization as determined from radon mass-balance measurements in the structure during advection experiments and by the numerical model using measured soil permeabilities as inputs. The vertical bars indicate the maximum and minimum estimates of entry based on uncertainty in the amount of non-slot, below-grade leakage, and propagation of error of measured parameters.

Table I. A comparison of soil air-permeability measurements made at 30 probes on the two dates with the highest and lowest average measured permeabilities. Multiply table values by 10^{-13} to obtain permeabilities in m^2. Uncertainties are dominated by environmental noise in the measured values of pressure and flow.

Measurement Date->	Oct. 1, 1991	Jan. 07, 1991
High-wall probes	Backfill Region	
E	29 ± 2.0	10. ± 0.7
S	37 ± 2.5	8.7± 0.6
W	30 ± 2.0	4.4± 1.4
N	26 ± 1.8	9.4± 0.7
Avg.	31	8.1
	Natural Soil	
E (medium)	22 ± 2.0	2.2± 0.5
S (medium)	18 ± 1.2	1.5± 0.2
W(long)	240 ±23.	69. ± 4.9
N(long)	28 ± 1.9	1.7± 0.3
Avg.	77	19
Mid-wall probes	Backfill Region	
E	20 ± 2.3	21. ± 2.9
S	30 ± 2.0	11. ± 0.8
W	17 ± 1.2	6.8± 0.5
N	20 ± 1.3	14. ± 1.0
Avg.	22	13
	Natural Soil	
E (med)	75 ± 5.4	41. ± 2.7
S (med)	91 ± 6.2	48. ± 3.8
W(long)	83 ± 5.7	40. ± 2.7
N(long)	100 ± 7.2	61. ± 4.5
Avg.	87	45
Low-wall probes	Backfill Region	
E	39 ± 5.4	42. ± 3.9
S	52 ± 8.9	49. ± 6.5
W	73 ±17.	89. ±12.
N	45 ± 5.2	49. ± 6.1
Avg.	52	57
	Natural Soil	
E (medium)	190. ±80.	160. ±47.
S (medium)	2.0± 0.3	5.9± 0.5
W(long)	35. ± 3.8	18. ± 1.7
N(long)	< 1.8	< 1.6
Avg.[a]	76	61

Sub-slab probes		
(short)	64. ± 4.6	73. ± 5.0
(short)	44. ± 3.0	43. ± 3.0
(medium)	< 1.8	< 1.6
(medium)	170. ±12	170. ±13.
(medium)	< 1.9	1.6± 0.2
(long)	11. ± 1.1	12. ± 1.3
Avg.(b)	72	75

(a) Only first three values included in average.
(b) First, second, third, and fifth values included in average.

Figure 1.

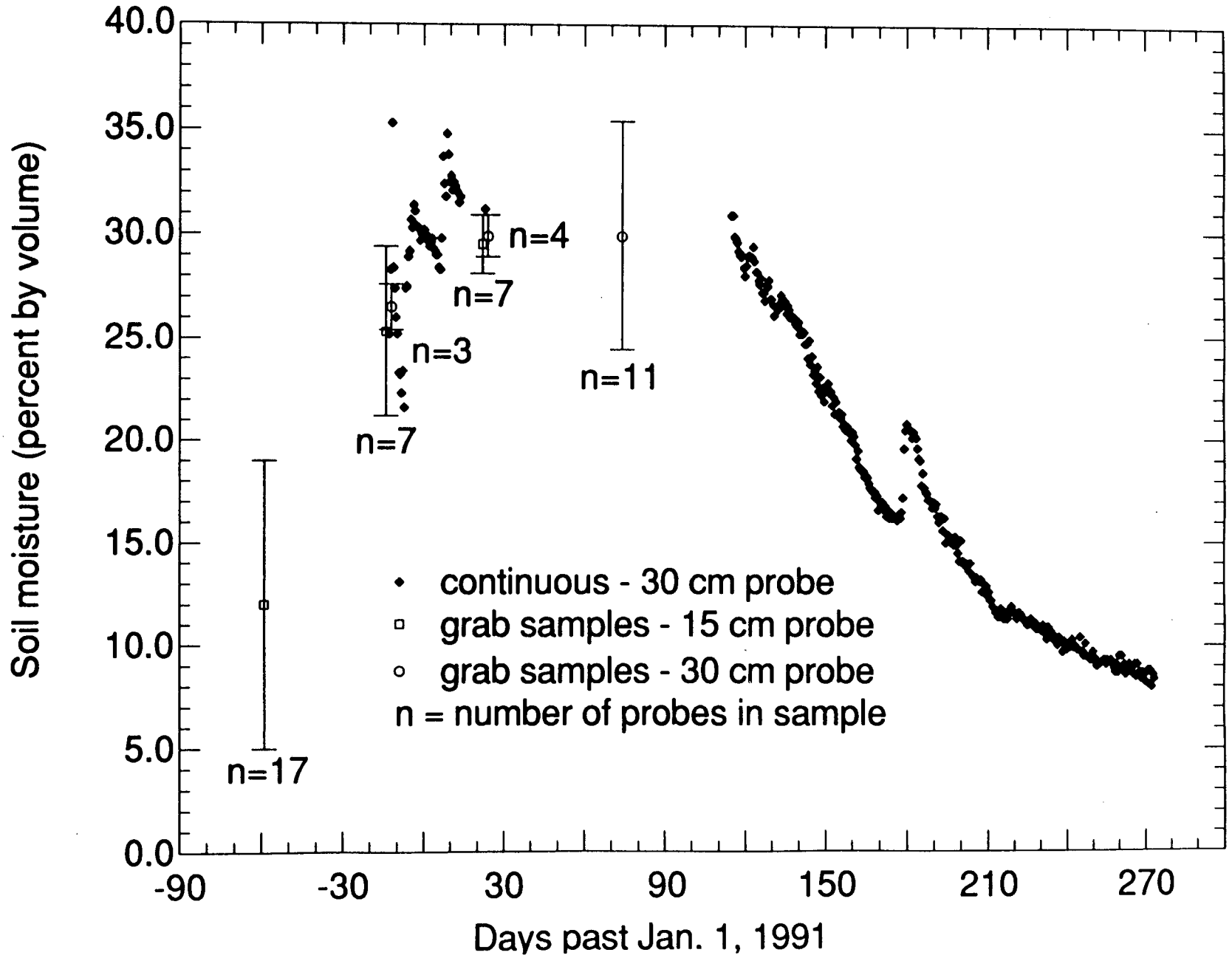
40.0
35.0
30.0
25.0
20.0
15.0
10.0
5.0
0.0
-90
-30
30
90
150
210
270
Soil moisture (percent by volume)
Days past Jan. 1, 1991
n=4
n=7
n=3
n=7
n=11
n=17
continuous - 30 cm probe
grab samples - 15 cm probe
grab samples - 30 cm probe
n = number of probes in sample

Figure 2.

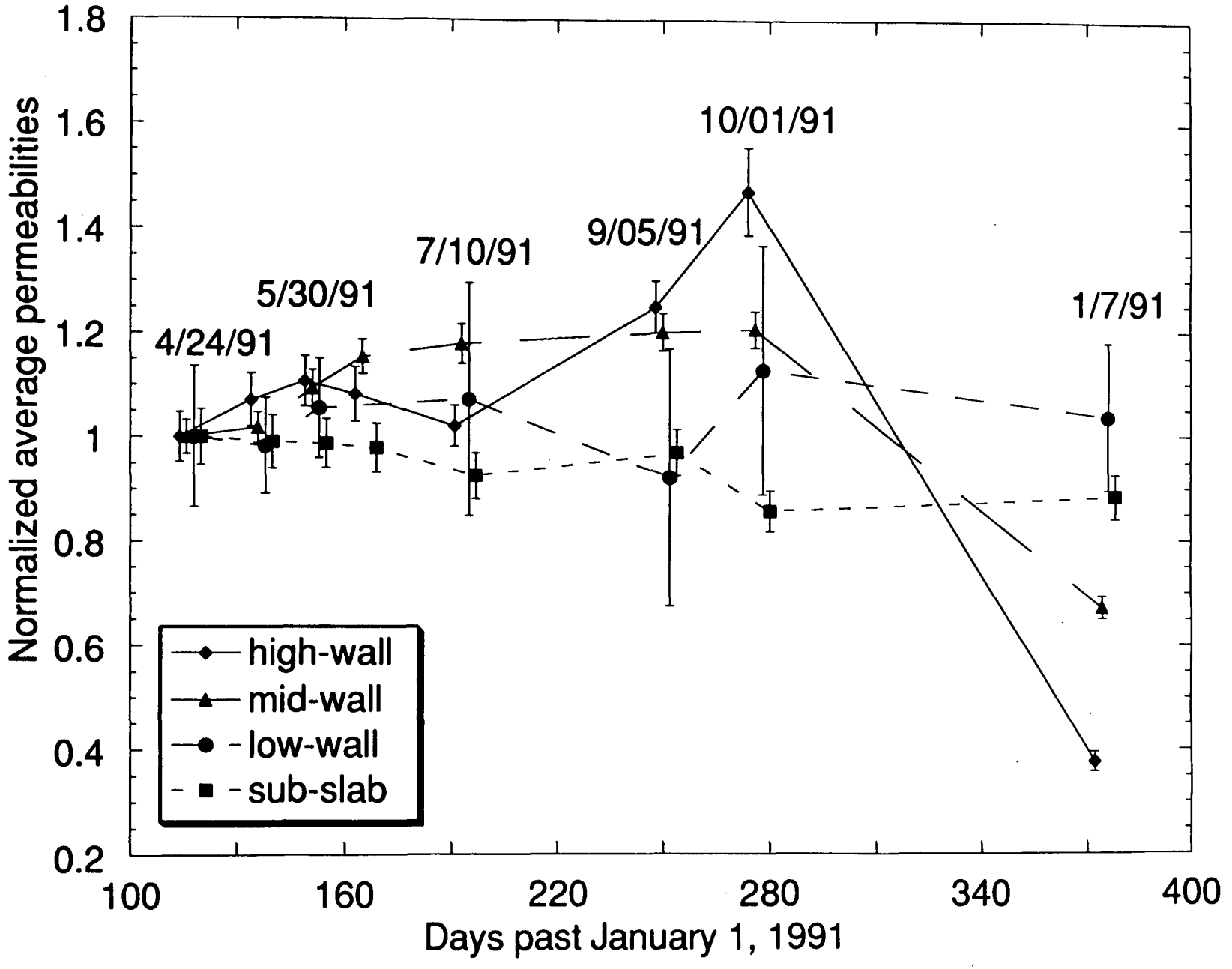
Normalized average permeabilities
1.8
1.6
1.4
1.2
1
0.8
0.6
0.4
0.2
100
160
220
280
340
400
Days past January 1, 1991
4/24/91
5/30/91
7/10/91
9/05/91
10/01/91
1/7/91
high-wall
mid-wall
low-wall
sub-slab

Figure 3.

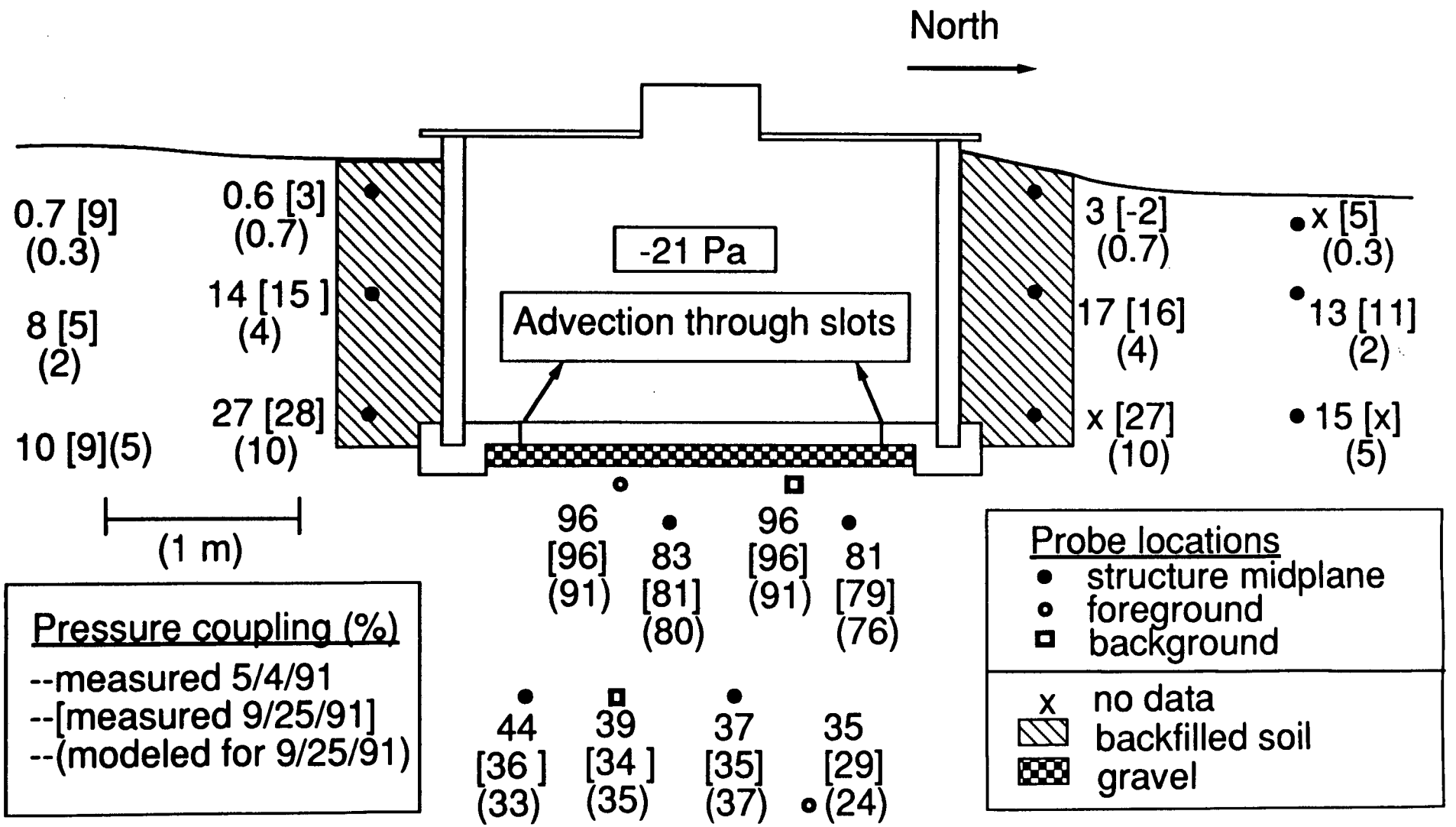
North
0.7 [9]
(0.3)
0.6 [3]
(0.7)
8 [5]
(2)
14 [15]
(4)
10 [9](5)
27 [28]
(10)
-21 Pa
Advection through slots
3 [-2]
(0.7)
x [5]
(0.3)
17 [16]
(4)
13 [11]
(2)
x [27]
(10)
15 [x]
(5)
(1 m)
96
[96]
(91)
83
[81]
(80)
96
[96]
(91)
81
[79]
(76)
44
[36]
(33)
39
[34]
(35)
37
[35]
(37)
35
[29]
(24)
Pressure coupling (%)
--measured 5/4/91
--[measured 9/25/91]
--(modeled for 9/25/91)
Probe locations
structure midplane
foreground
background
x no data
backfilled soil
gravel

Figure 4.

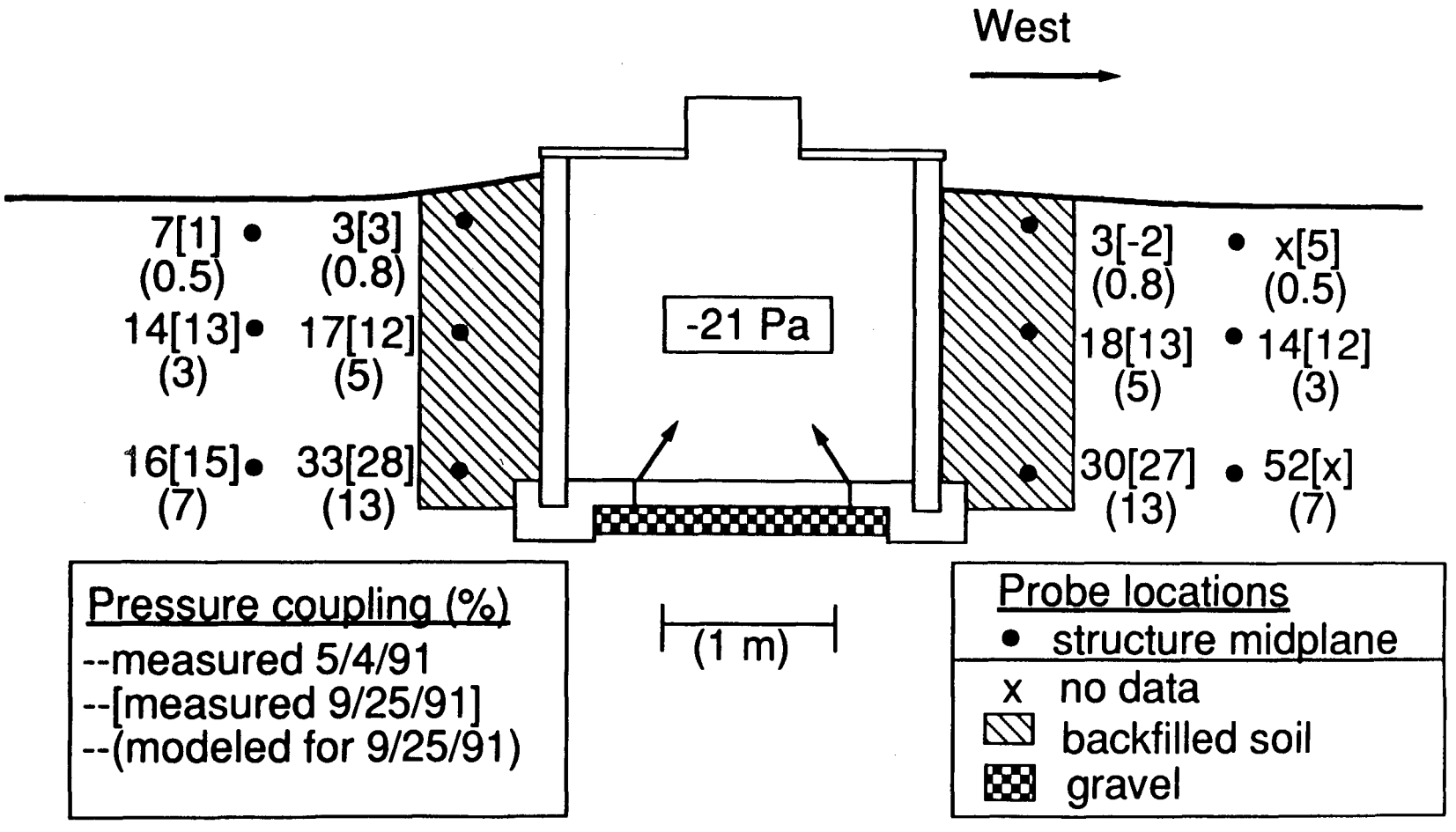
West
7[1]
(0.5)
3[3]
(0.8)
14[13]
(3)
17[12]
(5)
16[15]
(7)
33[28]
(13)
-21 Pa
3[-2]
(0.8)
x[5]
(0.5)
18[13]
(5)
14[12]
(3)
30[27]
(13)
52[x]
(7)
Pressure coupling (%)
--measured 5/4/91
--[measured 9/25/91]
--(modeled for 9/25/91)
(1 m)
Probe locations
structure midplane
x no data
backfilled soil
gravel

Figure 5.

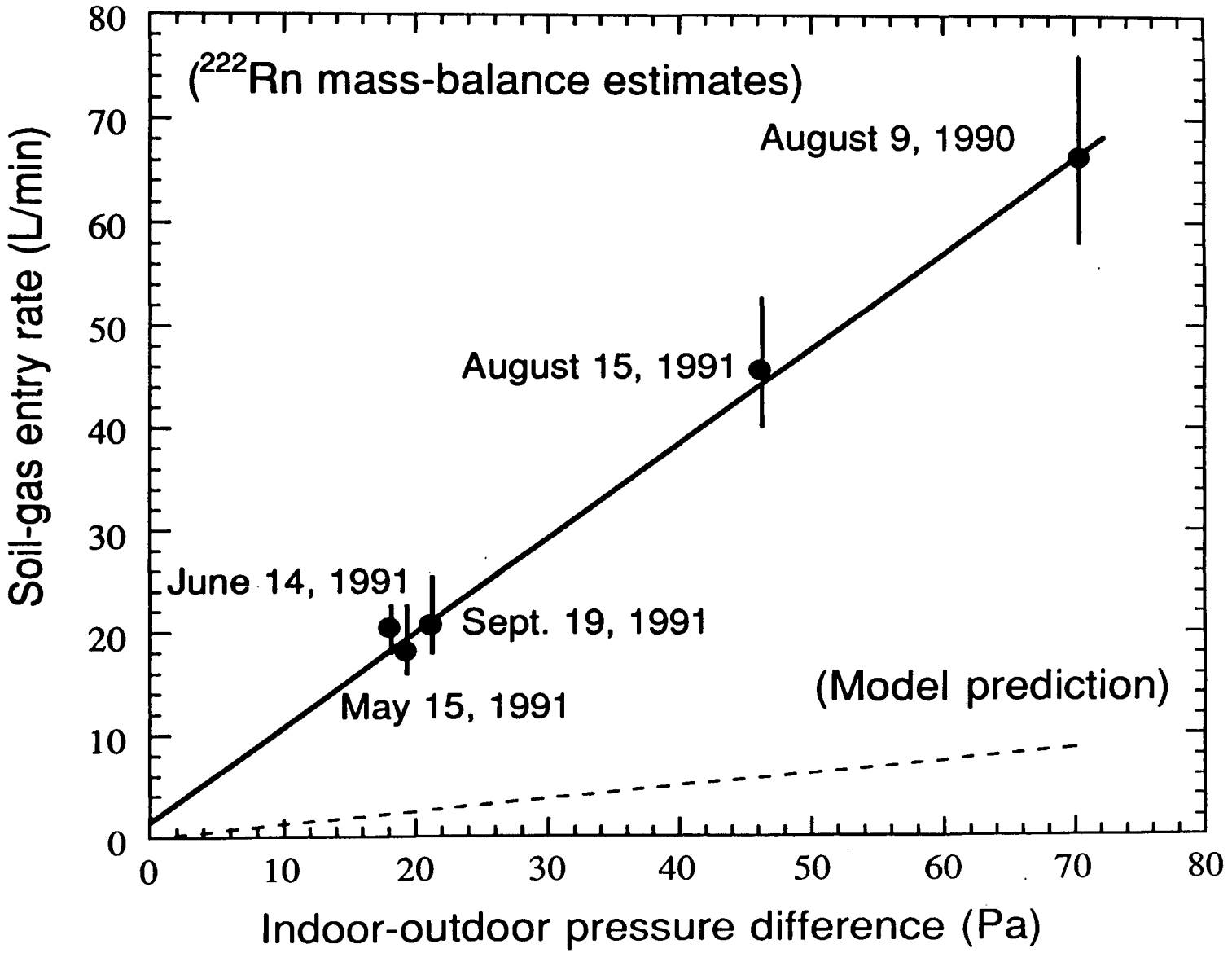
(222Rn mass-balance estimates)
August 9, 1990
August 15, 1991
June 14, 1991
Sept. 19, 1991
May 15, 1991
(Model prediction)
Soil-gas entry rate (L/min)
Indoor-outdoor pressure difference (Pa)
0
10
20
30
40
50
60
70
80

LAWRENCE BERKELEY LABORATORY
UNIVERSITY OF CALIFORNIA
TECHNICAL INFORMATION DEPARTMENT
BERKELEY, CALIFORNIA 94720